ADVANCED MATERIALS

Supporting Information

for *Adv. Mater.,* DOI: 10.1002/adma.202210834

Temperature-Dependent Reversal of Phase Segregation in Mixed-Halide Perovskites

*Adam D. Wright, Jay. B. Patel, Michael B. Johnston, and Laura M. Herz**

Supporting Information: Temperature-Dependent Reversal of Phase Segregation in Mixed-Halide Perovskites

Adam D. Wright[1], *Jay B. Patel*[1], *Michael B. Johnston*[1] *and Laura M. Herz*[1,2]*

Email: laura.herz@physics.ox.ac.uk

[1]Department of Physics, University of Oxford, Clarendon Laboratory, Parks Road, Oxford OX1 3PU, United Kingdom

[2] Institute for Advanced Study, Technical University of Munich (TUM), Lichtenbergstraße 2a, 85748 Garching bei München, Germany

Contents

S1. Sample fabrication methods

S1.1. $MAPb(Br_{0.4}I_{0.6})_3$ thin film samples

$CH_3NH_3Pb(Br_{0.4}I_{0.6})_3$ thin film samples were prepared using the acetonitrile route as reported previously[1,2] In summary, the precursor salts (methylammonium iodide, MAI, GreatCell Solar; methylammonium bromide, MABr, GreatCell Solar; lead iodide, PbI_2, TCI; lead bromide, $PbBr_2$, >98%, Alfa Aesar) were weighed stoichiometrically and dissolved in acetonitrile (Sigma Aldrich) to give a 0.5 M solution as described by Noel *et al.*[1].

Substrates made of z-cut quartz (area 1.3 cm^2) were cleaned by subsequent sonication in Decon90 (1 vol% in deionized water), deionized water, acetone (Sigma Aldrich) and isopropanol (Sigma Aldrich) for 10 min each. The substrates were then UV-Ozone treated for 10 minutes and then transferred into an N_2 filled glovebox prior to deposition of the perovskite layer.

The perovskite films were fabricated using the following procedure: 70 µl of precursor solution was statically deposited onto the quartz substrate which was then accelerated to 2000 rpm and maintained at 2000 rpm for 45 seconds. The films were then annealed for 30 min at 100 °C. PMMA (poly(methyl methacrylate), Sigma Aldrich, mean molar weight 97 000 g mol^{-1}) was dissolved in chlorobenzene (Sigma Aldrich) at 150 mg ml^{-1}. To form the PMMA film, 40 µl of solution was deposited dynamically onto the perovskite film at 2000 rpm, for 25 s. The films were then annealed at 100 °C for 1 min to drive off any residual solvent. The average film thickness was 810 nm as measured using a Bruker Dektak XTL Stylus profilometer.

S1.2. $MAPb(Br_{0.5}I_{0.5})_3$ thin film samples

Z-cut quartz was first cleaned using Hellmanex, acetone and isopropanol, then with oxygen plasma for 10 minutes.

The $MAPb(Br_{0.5}I_{0.5})_3$ perovskite was prepared using an adaptation of the procedure proposed by F. Huang *et al.* [3]. The perovskite films were prepared by dissolving the precursor salts in anhydrous N,N-dimethylformamide (DMF) and dimethyl sulfoxide (DMSO) mixture (4:1 volume ratio) to obtain a stoichiometric solution with the desired $MAPb(Br_{0.5}I_{0.5})_3$ composition. The precursor solution was prepared using the following precursor salts: (methylammonium iodide, MAI, GreatCell Solar; methylammonium bromide, MABr, GreatCell Solar; lead iodide, PbI_2, TCI; lead bromide, $PbBr_2$, >98%, Alfa Aesar). The perovskite precursor solution was spin coated from a 1.0 M solution at 4000 rpm for 30 seconds. N_2 gas was used to quench the growth of the perovskite. The gas flow was applied 15 seconds after the start of the spin coating, and sustained for 10 seconds. The perovskite films were immediately placed on a preheated hot plate set to 100 °C and annealed in a N_2 atmosphere for 20 minutes. Poly(methyl methacrylate) (PMMA) layer preparation: PMMA (Sigma Aldrich, average MW 97,000) was dissolved in chlorobenzene with a concentration of 150 mg mL^{-1}. The solution was spin coated at 2000 rpm for 45 seconds on top of the perovskite films.

The back of the quartz substrate was cleaned with isopropanol to ensure no residue at the back of the sample would interfere with measurements.

As measured previously using SEM cross-sectional images [4], the average perovskite layer thickness was found to be 390 nm and the average PMMA layer thickness to be 1300 nm.

S2. Photoluminescence spectroscopy methods

S2.1. Experimental setup

To measure the time-dependent steady-state photoluminescence (PL) of $MAPb(Br_{0.4}I_{0.6})_3$ thin films, the samples were photoexcited by a diode-pumped continuous wave laser (Spectra-Physics, Millennia Vis J) at a wavelength of 532 nm, which was attenuated with a combination of neutral density filters to result in excitation intensities ranging from 10 mW cm^{-2} to 300 W cm^{-2}. Meanwhile, the $MAPb(Br_{0.5}I_{0.5})_3$ films were photoexcited by a 398 nm diode laser (PicoHarp, LDH-D-C-405M). Continuous wave excitation with intensities ranging from 30 mW cm^{-2} to 40 W cm^{-2} were used. A fresh spot was used for each measurement [4].

The resultant PL was collected and coupled into a grating spectrometer (Princeton Instruments, SP-2558), which directed the spectrally dispersed PL onto a silicon iCCD (PI-MAX4, Princeton Instruments). The samples were mounted in either a gas-exchange helium cryostat (Oxford Instruments, OptistatCF2) in a helium atmosphere, or under vacuum (P<10^{-6} mbar) in a cold-finger liquid helium cryostat (Oxford Instruments, MicrostatHe).

The PL signal was attenuated before it reached the iCCD by manual change of neutral density filters in order to ensure that the detection signal fell into the linear regime. This was necessary since the iodide-rich phase is known to be associated with enhanced photoluminescence quantum yield compared to the mixed-halide phase, as a result of the charge-carrier concentration effect when electrons and holes are swept from the mixed majority phase into the segregated minority domains, leading to enhanced bimolecular electron-hole recombination [5]. The attenuation factor of the neutral density filters was accounted for when extracting the actual intensity of the PL emitted from the sample. Gaps in the data displayed in Figure 2 of the main manuscript correspond to time elapsed while the neutral density filters were changed, or periods when the signal at the iCCD detector became so large that it entered a nonlinear regime and/or saturated. We stress that this filter change occurred on the PL detection side only, thus leaving the excitation conditions and therefore the continued segregation process unaffected. The individual PL spectra collected at each time were normalized against their own maximum PL intensity within the energetic range covering both the mixed-halide peak and iodide-rich peak, which for the $MAPb(Br_{0.4}I_{0.6})_3$ thin films corresponded to a range of 1.51 to 1.98 eV.

The charge-carrier densities present under continuous illumination with different excitation intensities were estimated as follows. Illumination intensities were first calculated by dividing the incident power by the area of the circle defined by the Gaussian full width at half maximum of the laser beam. We further assumed that the excited charge carriers were distributed over a film depth of 500 nm, defined by the absorption coefficient of $MAPb(Br_{0.4}I_{0.6})_3$ of ~2×10^4 cm^{-1} at the excitation wavelength of 532 nm as reported by Hoke *et al.* [6]. Under the continuous-wave excitation with intensity 5 W cm^{-2}, these conditions result in a charge-carrier density generation rate of G=2.68 $\times10^{23}$ s^{-1} cm^{-3}. In the steady state, the generation rate equates to the charge-carrier recombination rate, according to $G=k_1 n + k_2 n^2 + k_3 n^3$, where k_1, k_2 and k_3 are the monomolecular (trap-related), bimolecular electron-hole and Auger recombination rate constants, respectively [7]. By solving the cubic equation using the rate constants we reported recently in Motti *et al.* [5] for lead mixed-halide perovskites made as part of the same batch as those used in the present study (i.e. $k_1 \approx 100 \times 10^6$ s^{-1}, $k_2 \approx 4 \times 10^{-9}$ cm^3 s^{-1} and $k_3 \approx 10^{-28}$ cm^6 s^{-1}), we obtain a charge-carrier density of 2.4×10^{15} cm^{-3} for excitation with intensity 5 W cm^{-2}, and analogously, charge-carrier densities of 1.6×10^{16} cm^{-3} and 5.2×10^{16} cm^{-3} for higher excitation intensities of 50 and 300 W cm^{-2}, respectively.

The charge-carrier density under continuous-wave excitation does not scale linearly with the generation rate, because higher-order processes, such as bimolecular and Auger recombination, become more dominant for higher generation rates. We note that a recent study [5] showed once these materials have suffered halide segregation, charge carriers funnel into iodide-rich domains within tens of picoseconds, where they subsequently recombine on the nanoseconds time scale. The transfer of heat to the lattice upon the relaxation of charge carriers from the mixed into the iodide-rich phase will therefore scale primarily with the excitation intensity.

S2.2. Parametrization of data

The intensity of the light emerging from the mixed-phase and iodide-rich perovskite regions was determined by integration over the two associated spectral regions, a method previously employed by Knight *et al.* [4]. These regions spanned a spectral bandwidth of 10 nm, centered on either the initial maximum PL intensity for the mixed-phase emission, or the final maximum PL intensity for the iodide-rich emission. The central wavelengths of the two emissions varied with temperature and excitation intensity.

The rate of halide segregation was parametrized by the 'switch-over time', t_{sw}, corresponding to the time at which the integrated PL intensity in the iodide-rich region exceeded that of the mixed-phase emission.

The progress of halide segregation under laser excitation was also tracked by means of calculating the average photon energy [8], $\langle E_{\mathrm{ph}} \rangle$, of the overall emission as defined by

$$\langle E_{\mathrm{ph}} \rangle = \frac{\int I(\lambda)\, \mathrm{d}\lambda}{\int I(\lambda) \frac{\lambda}{hc}\, \mathrm{d}\lambda}$$

where $I(\lambda)$ is the photoluminescence intensity.

S2.3. Atmospheric conditions

The temperature-dependent PL measurements for $MAPb(Br_{0.4}I_{0.6})_3$ were measured with thin films under a helium atmosphere in a gas-exchange cryostat for temperatures $\leq$250 K, and under vacuum in a cold-finger cryostat for temperatures $\geq$250 K. The gas-exchange cryostat was employed at low temperatures because the immersion of the sample in helium gas avoids the thermal contact difficulties involved in using cold-finger cryostats with metal halide perovskites, which have very low thermal conductivity [9,10], thus rendering a highly accurate setting of sample temperature. However, the indium seals in the gas-exchange cryostat prevented its usage at high temperatures where such seals disintegrate. The switch-over times determined from the two datasets recorded with both methods at the 250 K overlap temperature agreed to within experimental error, and Figure 2a of the main text shows the mean t_{sw} recorded with the two configurations.

As indicated in Figure S1, three temperature-dependent PL datasets were also taken for $MAPb(Br_{0.5}I_{0.5})_3$. Two of these were measured with the sample in the cold-finger cryostat across the full temperature range, while one was measured with the sample in the gas-exchange cryostat across the full temperature range. There was no discontinuity at 250 K for any of these datasets, nor was there a substantial difference between the t_{sw} derived from samples measured in different atmospheric conditions. We thus conclude that the presence or absence of an inert environmental gas has no impact on the measured data.

S3. Temperature dependence of switch-over time in $MAPb(Br_{0.5}I_{0.5})_3$

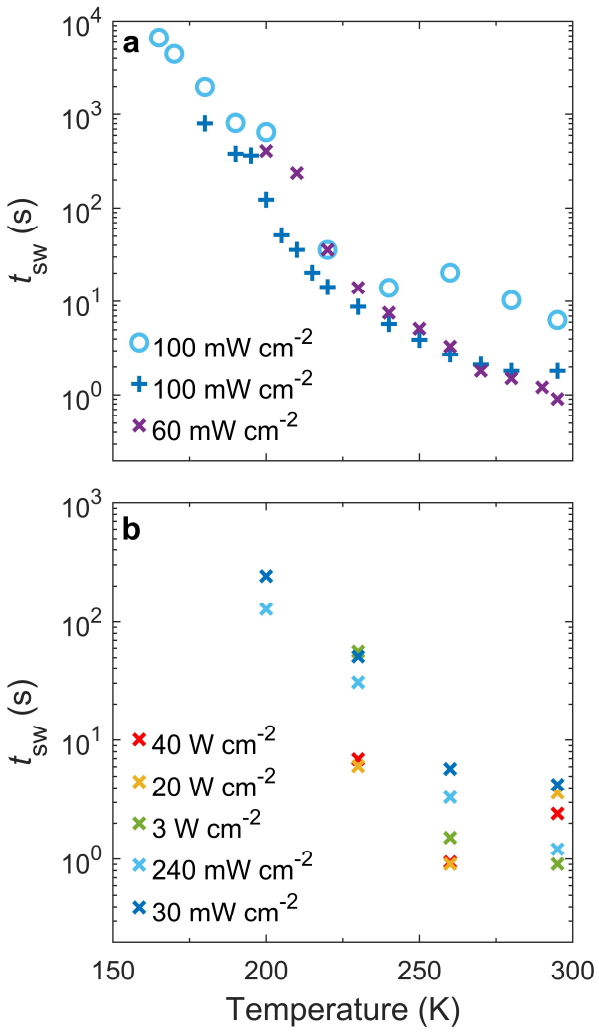

Figure S1: a) Temperature dependence of the switch-over time, t_{sw}, for $MAPb(Br_{0.5}I_{0.5})_3$ thin films excited at a wavelength of 398 nm by light intensities of around 1 sun. The light blue and dark blue datasets were collected on bare (uncoated) films measured in a cold-finger cryostat, whereas the purple data set was collected on a film coated with PMMA measured in a gas-exchange cryostat. The switch-over times of the PL spectra measured from this latter sample are shown in **b)** for a range of excitation intensities.

S4. Comparison of remixing data with previously reported data

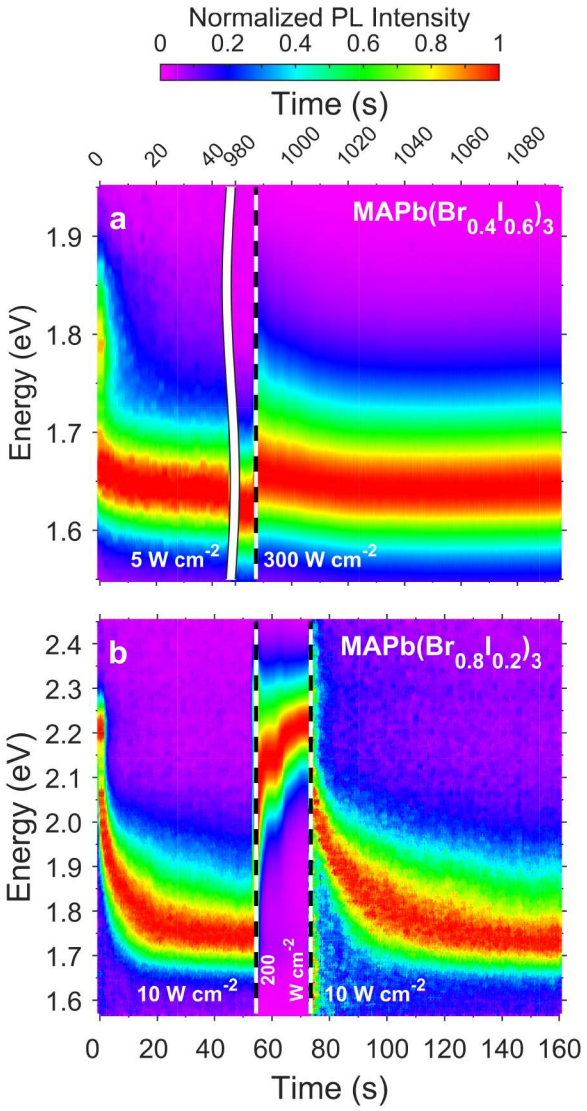

Figure S2: a) Normalized PL emission from $MAPb(Br_{0.4}I_{0.6})_3$ recorded under first 5, then 300 W cm^{-2} excitation intensity (with an intervening period under 50 W cm^{-2} intensity; full data shown in Figure 3a of the main text) at 295 K, using a 532 nm continuous-wave laser; compared with **b)** that shown in Figure 1a of Mao *et al*. [11] for $MAPb(Br_{0.8}I_{0.2})_3$ under excitation with intensity of first 10, then 200, then 10 W cm^{-2}. Note that we introduced an x-axis break in panel (a) to account for the longer duration under the initial low-intensity excitation and allow for ease of comparison. The dashed black-and-white lines indicate the transitions between the different excitation intensities. As with Mao *et al.*, we find that high-intensity excitation remixes the material and blueshifts its emission, but what we observe is less pronounced and more transient than them. Although the data of Mao *et al.* shown above was collected under excitation by a 400 nm pulsed laser, they also reported inducing similarly dramatic reversal of halide segregation using a 532 nm continuous-wave laser at an excitation intensity of only 10 W cm^{-2}.

[Figure S2b adapted by permission from Springer Nature Customer Service Centre GmbH: Springer Nature, Nature Materials [11]. W. Mao *et al.*, Light-induced reversal of ion segregation in mixed-halide perovskites, (20), 55–61, Copyright 2021]

S5. Comparison of remixing data recorded at different temperatures

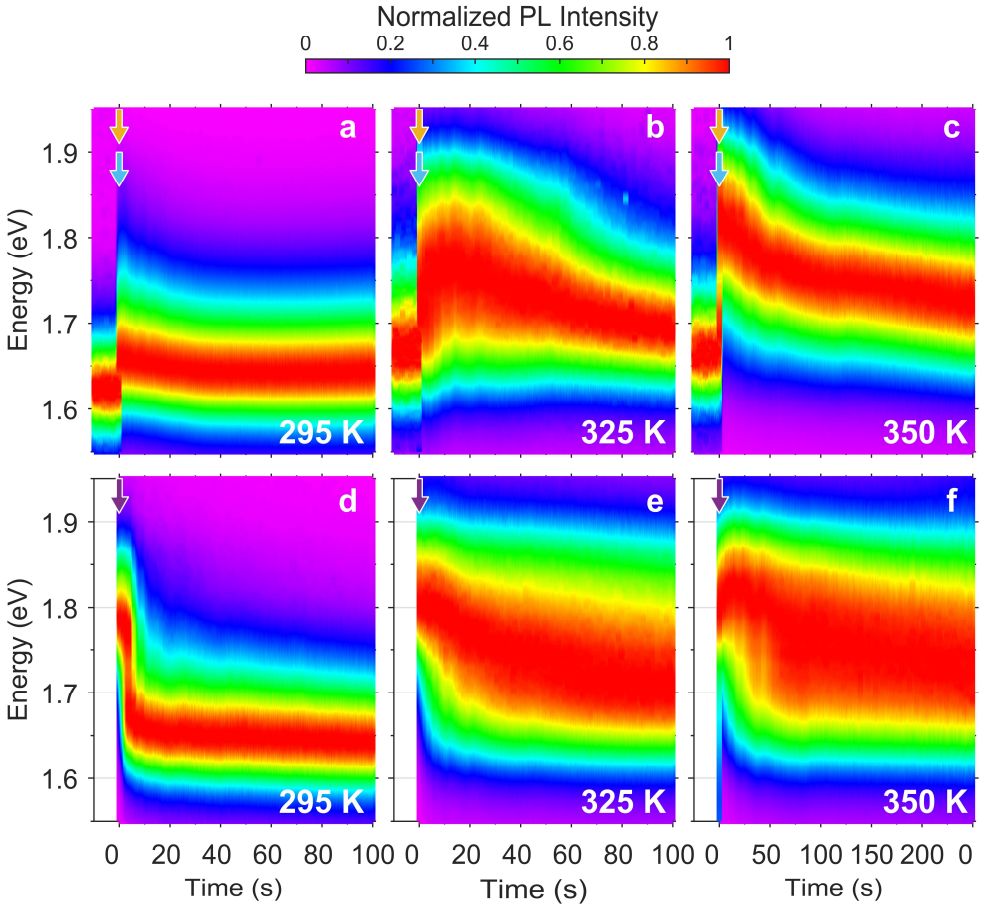

Figure S3: Normalized PL emission from $MAPb(Br_{0.4}I_{0.6})_3$ at **a,d)** 295 K, **b,e)** 325 K and **c,f)** 350 K placed under an excitation intensity of 300 W cm^{-2} (wavelength: 532 nm) from the point in time marked as zero. In **a)**, **b)** and **c)** the sample spots had been excited by 5 W cm^{-2} immediately prior to t = 0 (with an intervening period under 50 W cm^{-2} intensity as shown in Figure 3 of the main text) whereas in **d)**, **e)** and **f)** the sample spots were pristine (i.e. not exposed to excitation prior to time zero). Therefore, **a)**, **b)** and **c)** capture the mixed-halide film in a phase-segregated state at t = 0, with emission mostly originating from the iodide-rich phase, and an intensity-increase to 300 W cm^{-2} triggers halide re-mixing, while for **d)**, **e)** and **f)** the films are in a pristine well-mixed state at t = 0 and illumination with 300 W cm^{-2} initiates halide segregation. The arrows indicate the times at which the correspondingly colored spectra in Figure S4 were taken.

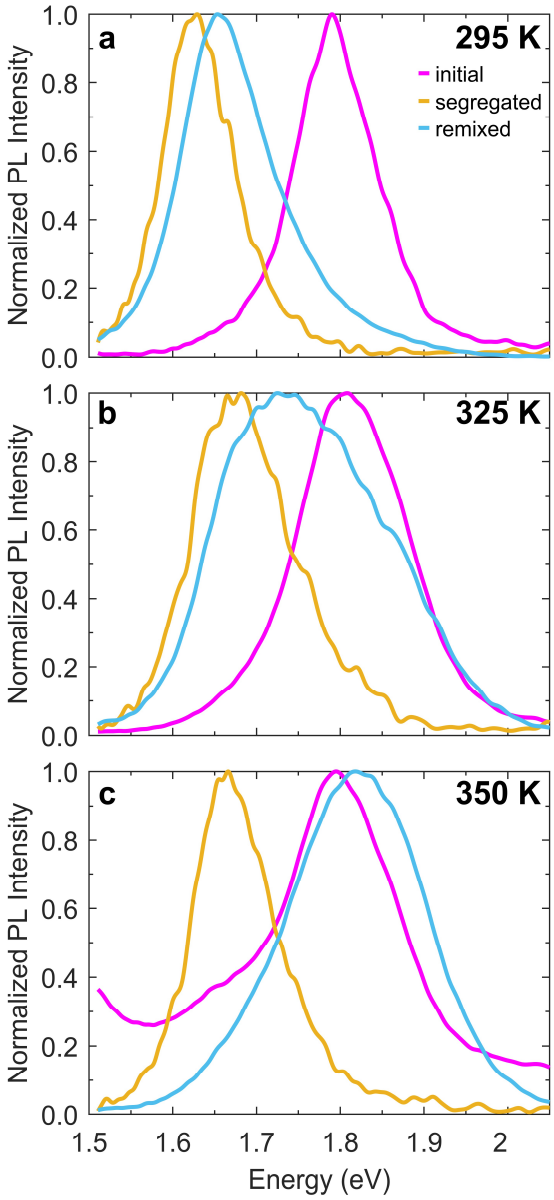

Figure S4: Normalized PL spectra from $MAPb(Br_{0.4}I_{0.6})_3$ at **a)** 295 K, **b)** 325 K and **c)** 350 K, sampled from the color maps in Figure S3 at the times indicated by the correspondingly colored arrows in that figure. The magenta spectra were taken on pristine sample spots at times immediately after the initial 5 W cm^{-2} excitation has been turned on, reflecting the well-mixed state of the system. The other spectra were taken on sample spots that had been excited by 5 W cm^{-2} intensity (with an intervening period under 50 W cm^{-2} intensity as shown in Figure 3 of the main text), just before (gold) and after [i.e. within 1 s] (light blue) the application of the 300 W cm^{-2} excitation. Here the gold curve shows how prolonged exposure to 5 W cm^{-2} illumination has led to red-shifted emission from iodide-rich domains, while the light blue curve illustrates how sudden application of 300 W cm^{-2} excitation reverts the films towards a mixed-halide state, in particular at higher temperatures.

References

(1) Noel, N. K.; Habisreutinger, S. N.; Wenger, B.; Klug, M. T.; Hörantner, M. T.; Johnston, M. B.; Nicholas, R. J.; Moore, D. T.; Snaith, H. J. A Low Viscosity, Low Boiling Point, Clean Solvent System for the Rapid Crystallisation of Highly Specular Perovskite Films. *Energy Environ. Sci.* **2017**, *10*, 145–152.

(2) Knight, A. J.; Borchert, J.; Oliver, R. D. J.; Patel, J. B.; Radaelli, P. G.; Snaith, H. J.; Johnston, M. B.; Herz, L. M. Halide Segregation in Mixed-Halide Perovskites: Influence of A-Site Cations. *ACS Energy Lett.* **2021**, *6*, 799–808.

(3) Huang, F.; Dkhissi, Y.; Huang, W.; Xiao, M.; Benesperi, I.; Rubanov, S.; Zhu, Y.; Lin, X.; Jiang, L.; Zhou, Y.; Gray-Weale, A.; Etheridge, J.; McNeill, C. R.; Caruso, R. A.; Bach, U.; Spiccia, L.; Cheng, Y.-B. Gas-Assisted Preparation of Lead Iodide Perovskite Films Consisting of a Monolayer of Single Crystalline Grains for High Efficiency Planar Solar Cells. *Nano Energy* **2014**, *10*, 10–18.

(4) Knight, A. J.; Wright, A. D.; Patel, J. B.; McMeekin, D. P.; Snaith, H. J.; Johnston, M. B.; Herz, L. M. Electronic Traps and Phase Segregation in Lead Mixed-Halide Perovskite. *ACS Energy Lett.* **2019**, *4*, 75–84.

(5) Motti, S. G.; Patel, J. B.; Oliver, R. D. J.; Snaith, H. J.; Johnston, M. B.; Herz, L. M. Phase Segregation in Mixed-Halide Perovskites Affects Charge-Carrier Dynamics While Preserving Mobility. *Nat. Commun.* **2021**, *12*, 6955.

(6) Hoke, E. T.; Slotcavage, D. J.; Dohner, E. R.; Bowring, A. R.; Karunadasa, H. I.; McGehee, M. D. Reversible Photo-Induced Trap Formation in Mixed-Halide Hybrid Perovskites for Photovoltaics. *Chem. Sci.* **2015**, *6*, 613–617.

(7) Johnston, M. B.; Herz, L. M. Hybrid Perovskites for Photovoltaics: Charge-Carrier Recombination, Diffusion, and Radiative Efficiencies. *Acc. Chem. Res.* **2016**, *49*, 146–154.

(8) Rehman, W.; McMeekin, D. P.; Patel, J. B.; Milot, R. L.; Johnston, M. B.; Snaith, H. J.; Herz, L. M. Photovoltaic Mixed-Cation Lead Mixed-Halide Perovskites: Links Between Crystallinity, Photo-Stability and Electronic Properties. *Energy Environ. Sci.* **2017**, *10*, 361–369.

(9) Xia, C. Q.; Peng, J.; Poncé, S.; Patel, J. B.; Wright, A. D.; Crothers, T. W.; Rothmann, M. U.; Borchert, J.; Milot, R. L.; Kraus, H.; Lin, Q.; Giustino, F.; Herz, L. M.; Johnston, M. B. Limits to Electrical Mobility in Lead-Halide Perovskite Semiconductors. *J. Phys. Chem. Lett.* **2021**, *12*, 3607–3617.

(10) Pisoni, A.; Jaćimović, J.; Barišić, O. S.; Spina, M.; Gaál, R.; Forró, L.; Horváth, E. Ultra-Low Thermal Conductivity in Organic-Inorganic Hybrid Perovskite $CH_3NH_3PbI_3$. *J. Phys. Chem. Lett.* **2014**, *5*, 2488–2492.

(11) Mao, W.; Hall, C. R.; Bernardi, S.; Cheng, Y.-B.; Widmer-Cooper, A.; Smith, T. A.; Bach, U. Light-Induced Reversal of Ion Segregation in Mixed-Halide Perovskites. *Nat. Mater.* **2021**, *20*, 55–61.